THE FASEB JOURNAL • RESEARCH • www.fasebj.org

The tumor secretory factor ZAG promotes white adipose tissue browning and energy wasting

Sawsan Elattar, Manali Dimri, and Ande Satyanarayana[1]
Department of Biochemistry and Molecular Biology, Georgia Cancer Center, Augusta University, Augusta, Georgia, USA

ABSTRACT: Cachexia is a complex tissue-wasting syndrome characterized by inflammation, hypermetabolism, increased energy expenditure, and anorexia. Browning of white adipose tissue (WAT) is one of the significant factors that contribute to energy wasting in cachexia. By utilizing a cell implantation model, we demonstrate here that the lipid mobilizing factor zinc-α_2-glycoprotein (ZAG) induces WAT browning in mice. Increased circulating levels of ZAG not only induced lipolysis in adipose tissues but also caused robust browning in WAT. Stimulating WAT progenitors with ZAG recombinant protein or expression of ZAG in mouse embryonic fibroblasts (MEFs) strongly enhanced brown-like differentiation. At the molecular level, ZAG stimulated peroxisome proliferator–activated receptor γ (PPARγ) and early B cell factor 2 expression and promoted their recruitment to the PR/SET domain 16 (Prdm16) promoter, leading to enhanced expression of Prdm16, which determines brown cell fate. In brown adipose tissue, ZAG stimulated the expression of PPARγ and PPARγ coactivator 1α and promoted recruitment of PPARγ to the uncoupling protein 1 (Ucp1) promoter, leading to increased expression of Ucp1. Overall, our results reveal a novel function of ZAG in WAT browning and highlight the targeting of ZAG as a potential therapeutic application in humans with cachexia.—Elattar, S., Dimri, M., Satyanarayana, A. The tumor secretory factor ZAG promotes white adipose tissue browning and energy wasting. FASEB J. 32, 4727–4743 (2018). www.fasebj.org

KEY WORDS: cachexia · beige adipocyte · Ebf2 · Prdm16 · Ucp1

Cachexia is a complex condition of tissue wasting that affects up to 80% of cancer patients. Of the different cancer types, cachexia occurs predominantly in gastrointestinal, pancreatic, and lung cancers (1). In addition to cancer, other end-stage diseases such as AIDS, congestive heart failure, rheumatoid arthritis, tuberculosis, and cystic fibrosis are also associated with cachexia (1). Patients with cachexia experience progressive loss of white adipose tissue (WAT) and skeletal muscle. This is due to systemic inflammation, hypermetabolism, increased resting energy expenditure, and anorexia. In cachexia, body energy balance and nutritional status are highly compromised. The body continuously senses a lack of nutrition that results in unwanted tapping into other sources of energy such as skeletal muscle and adipose tissue. Hypermetabolic activity and energy wasting in cachexia are predominantly caused by futile metabolic cycling such as glucose recycling between the liver and tumor (Cori cycle—glucose–lactate–glucose), and excessive lipid and protein turnover in the body (2, 3). Tumors secrete an array of cytokines such as TNF-α, IL-1, IL-6, IFN-γ, and proteolysis-inducing factor that have been implicated in altering metabolism and promoting cachexia. These factors trigger the onset of tissue wasting by altering multiple pathways for energy metabolism (2, 3). Some of these factors, such as TNF-α and IL-6, have been shown to induce cachexia-like effects when administered even in the absence of tumors (4–6).

Another factor that significantly contributes to energy wasting in cachexia is browning of WAT (7, 8). There are 2 different types of adipose tissue in the body, WAT and brown adipose tissue (BAT), which perform physiologically opposite functions. WAT is responsible for storing extra energy in the form of triglycerides,

ABBREVIATIONS: aP2, adipocyte protein 2; BAT, brown adipose tissue; CEBP, CCAAT enhancer binding protein; ChIP, chromatin immunoprecipitation; CideA, cell death–inducing DFFA-like effector A; Cox, cytochrome *c* oxidase; Dio2, iodothyronine deiodinase 2; dT, dTomato; Ebf2, early B cell factor 2; eWAT, epididymal white adipose tissue; H&E, hematoxylin and eosin; HEK-293, human embryonic kidney 293; IRF4, IFN regulatory factor 4; iWAT, inguinal white adipose tissue; MEF, mouse embryonic fibroblast; PGC1α, peroxisome proliferator–activated receptor γ coactivator 1α; PPARγ, peroxisome proliferator–activated receptor γ; Prdm16, PR/SET domain 16; PTGS2, prostaglandin-endoperoxide synthase 2; PTHLH, parathyroid hormone–like hormone; qPCR, quantitative PCR; SRC1, steroid receptor coactivator 1; SVF, stromal vascular fraction; Ucp1, uncoupling protein 1; WAT, white adipose tissue; ZAG, zinc-α_2-glycoprotein; β3-AR, β3-adrenergic receptor

[1] Correspondence: Augusta University, 1410 Laney Walker Blvd., Room-CN3150, Augusta, GA 30912, USA. E-mail: sande@augusta.edu

doi: 10.1096/fj.201701465RR
This article includes supplemental data. Please visit *http://www.fasebj.org* to obtain this information.

whereas BAT dissipates energy as heat under certain physiologic conditions (9). In addition to the interscapular BAT, brown-like adipocytes can also be generated within WAT, a phenomenon called WAT browning, and the brown-like adipocytes are termed "beige" or "brite" adipocytes. Beige adipocytes are derived from the adipose progenitor/precursor cells (10), where early B cell factor 2 (Ebf2) and peroxisome proliferator–activated receptor γ (PPARγ) cooperatively induce the expression of *PR/SET domain 16* (*Prdm16*), which stimulates beige adipocyte differentiation (11–13). Induced expression of *Prdm16* or *Ebf2* is sufficient to convert white adipose precursors into brown-like cells that express uncoupling protein 1 (Ucp1) in both *in vitro* and *in vivo* settings (11, 14–16). Similar to brown adipocytes, beige adipocytes also consume glucose and fatty acids and dissipate energy as heat by uncoupled respiration. Both brown and beige adipocytes express high levels of Ucp1, which facilitates uncoupled respiration and increases energy expenditure (17). WAT browning has been known to occur not only in mouse models of cachexia but also in human cachexia patients (7).

Zinc-α_2-glycoprotein (ZAG) is a ~41 kDa soluble protein first isolated from human plasma (18). ZAG is highly expressed in breast, prostate, lung, and bladder tumors, among others, and its expression level is elevated in the serum of cancer patients (19–22). ZAG has been identified as a lipid mobilizing factor that promotes lipolysis and inhibits lipogenesis in WAT (23, 24). Later studies have shown that the expression and circulating levels of ZAG are inversely correlated to adiposity. ZAG mRNA and protein expression are decreased or lost in adipose tissues of obese mice and patients (25, 26). ZAG stimulates lipolysis in adipocytes *via* activation of β3-adrenergic receptors (β3-ARs) and activation of the cAMP pathway (27). However, whether ZAG plays any role beyond lipolysis or participates in other energy-wasting mechanisms of cachexia such as WAT browning has not been explored. By utilizing ZAG-expressing cell implantation models, we demonstrate here that ZAG not only induces lipolysis in the WAT of mice but also promotes WAT browning.

MATERIALS AND METHODS

Mice and diet

Mice were housed in a specific pathogen-free barrier facility under standard conditions with a 12-h light/dark cycle. Mice were handled in compliance with the *Guide for the Care and Use of Laboratory Animals* (National Institutes of Health, Bethesda, MD, USA). All animal protocols were reviewed and approved by the Institutional Animal Care and Use Committee of Augusta University. Athymic nude mice (#490) were purchased from Charles River Laboratories (Wilmington, MA, USA). C57BL/6J mice (#000664) were purchased from The Jackson Laboratory (Bar Harbor, ME, USA). Mice were fed a standard chow diet containing 6% crude fat (Harlan Teklad Rodent Diet 2918; Envigo, Huntingdon, United Kingdom).

Subcutaneous cell implantation in mice

For subcutaneous cell implantation experiments, 1×10^8 dTomato (dT) tag, ZAG-dT, ZAG-expressing mouse embryonic fibroblasts (MEFs), or human embryonic kidney 293 (HEK-293) cells were implanted subcutaneously in the flank region. MEFs were implanted in 8–10-wk-old athymic nude mice. Mice were euthanized 3 and 6 wk after cell implantation, and different tissues and blood were collected for further analyses.

In vivo multispectral optical imaging

Multispectral optical images were acquired 3 and 6 wk after cell implantation using excitation and emission profiles of 570 and 610 nm to monitor dT-positive cells and circulating dT-ZAG in athymic nude mice. All optical imaging data were acquired through the use of Spectral AMI equipment and analyzed using its accompanying AMIView Image Analysis Software (Spectral Instruments Imaging, Tucson, AZ, USA).

Brown adipocyte differentiation in WAT progenitors and MEFs

The stromal vascular fraction (SVF) from the WAT of 7–8-wk-old C57BL/6J mice was isolated and cultured, and the white adipose progenitors were differentiated into brown adipocytes as previously described (13). The adipocyte differentiation medium was supplemented with 1 μg/ml ZAG recombinant protein (4764-ZA; R&D Systems, Minneapolis, MN, USA) or vehicle (PBS), and the differentiated cells were collected at different time points. We also generated vector control and ZAG-expressing stable immortalized MEF cell lines. MEFs were cultured in 100 mm dishes and induced to differentiate into brown adipocytes as previously described (12, 28). The differentiated cells were collected at different time points for further analysis.

Real-time quantitative PCR

Total RNA from cells and tissues were prepared using Trizol Reagent (15596-026; Thermo Fisher Scientific, Waltham, MA, USA) according to the manufacturer's instructions. Total RNA (1 μg) from each sample was reverse transcribed into cDNA using the RevertAid RT Kit (K1691; Thermo Fisher Scientific) according to the manufacturer's instructions. Quantitative PCR (qPCR) analysis was performed using Power SYBR Green PCR Master Mix (4367659; Thermo Fisher Scientific) according to the manufacturer's instructions in a 20-μl final reaction volume in 96-well plates (4346907; Thermo Fisher Scientific). The qPCR primers used are provided in **Table 1**.

Luciferase reporter assays

The *Prdm16* and *Ucp1* promoter–driven luciferase reporter assays were performed as previously described (28). *Prdm16* luciferase assays were performed using the C2C12 mouse myoblast cell line, which has no endogenous Ebf2 activity, and *Ucp1* luciferase reporter assays were carried out using the Cos7 African green monkey kidney fibroblast–like cell line.

Chromatin immunoprecipitation–qPCR

PPARγ/Prdm16 promoter, Ebf2/Prdm16 promoter and PPARγ/Ucp1 promoter chromatin immunoprecipitation (ChIP)–qPCR

TABLE 1. *Mouse primers used for real-time qPCR and ChIP-qPCR*

Gene	Primer, 5′–3′	
	Forward	Reverse
ZAG	GGACACTACAGGGTCTCACACCTT	TGAAATCCTCTCCGTCGTAGGC
Ap2	ACACCG AGATTTCCTTCAAACTG	CCATCTAGGGTTATGATGCTCTTCA
CideA	TGCTCTTCTGTATCGCCCAGT	GCCGTGTTAAGGAATCTGCTG
Dio2	CAGTGTGGTGCACGTCTCCAATC	TGAACCAAAGTTGACCACCAG
Pgc1α	CCCTGCCATTGTTAAGACC	TGCTGCTGTTCCTGTTTTC
SRC1	TTTCAAGAAGTGATGACTCGTGG	CCAGGATTGACTGAGGGATT
Pparγ	GTGCCAGTTTCGATCCGTAGA	GGCCAGCATCGTGTAGATGA
Prdm16	CAGCACGGTGAAGCCATTC	GCGTGCATCCGCTTGTG
Ebf2	GCTGCGGGAACCGGAACGAGA	ACACGACCTGGAACCGCCTCA
Ucp1	ACTGCCACACCTCCAGTCATT	CTTTGCCTCACTCAGGATTGG
Elovl3	TCCGCGTTCTCATGTAGGTCT	GGACCTGATGCAACCCTATGA
Nrf1	GAACTGCCAACCACAGTCAC	TTTGTTCCACCTCTCCATCA
Nrf2	GCTTTTGGCAGAGACATTCC	ATCAGCCAGCTGCTTGTTTT
Essrα	TTCTGCACAGCTTCCACATC	GGAAGAATTCGTCACCCTCA
Cycs	GCAAGCATAAGACTGGACCAAA	TTGTTGGCATCTGTGTAAGAGAATC
Cpt1b	CGAGGATTCTCTGGAACTGC	GGTCGCTTCTTCAAGGTCTG
Cox3	GCAGGATTCTTCTGAGCGTTCT	GTCAGCAGCCTCCTAGATCATGT
Cox4	ACCAAGCGAATGCTGGACAT	GGCGGAGAAGCCCTGAA
Cox5b	GCTGCATCTGTGAAGAGGACAAC	CAGCTTGTAATGGGTTCCACAGT
Cox7a	CAGCGTCATGGTCAGTCTGT	AGAAAACCGTGTGGCAGAGA
Cox8b	GAACCATGAAGCCAACGACT	GCGAAGTTCACAGTGGTTCC
CD40	TTGTTGACAGCGGTCCATCTA	CCATCGTGGAGGTACTGTTTG
Tnfrsf9	CGTGCAGAACTCCTGTGATAAC	GTCCACCTATGCTGGAGAAGG
Tbx1	GGCAGGCAGACGAATGTTC	TTGTCATCTACGGGCACAAAG
Tmem26	ACCCTGTCATCCCACAGAG	TGTTTGGTGGAGTCCTAAGGTC
Mouse 18S rRNA	GTAACCCGTTGAACCCCATT	CCATCCAATCGGTAGTAGCG
Prdm16-ChIP	GACCTCCTGCCTTCCCTGAGG	GCTGCCTGAGCTGGGCCAGCC
Ucp1-ChIP	AGTGAAGCTTGCTGTCACTC	GTCTGAGGAAAGGGTTGACC
18s-ChIP	AGTCCCTGCCCTTTGTACACA	CGATCCGAGGGCCTCACT

Elovl3, ELOVL fatty acid elongase 3; Nrf1/Nrf2, nuclear respiratory factor 1/2; *Esrα*, estrogen-related receptor α; *Cycs*, cytochrome *c*, somatic; *Cpt1b*, carmitine palmitoyltransferase 1b; *Tnfrsf9*, TNF receptor superfamily member 9; *Tbx1*, T-box 1; *Tmem26*, transmembrane protein 26.

assays were performed as previously described (13, 28) using the ChIP Assay Kit (17-295; MilliporeSigma, Burlington, MA, USA). dT control and ZAG-expressing MEFs were differentiated for 5 d and used for ChIP-qPCR assays. Primer sequences are provided in Table 1.

Prostaglandin-endoperoxide synthase 2 activity assay

Prostaglandin-endoperoxide synthase 2 (PTGS2) enzymatic activity in eWAT (epididymal WAT) lysates was measured using the Cyclooxygenase [Cytochrome *c* Oxidase (COX)] Activity Assay Kit according to the manufacturer's instructions (ab204699; Abcam, Cambridge, United Kingdom).

ZAG, IL-6, TNF-α, and parathyroid hormone–related protein ELISAs

For ZAG, IL-6, TNF-α, and parathyroid hormone–like hormone (PTHLH) measurements, blood serum was prepared, divided into aliquots, and stored at −80°C until use. ZAG concentration was determined by mouse ZAG ELISA Kit (MBS027874; MyBioSource, San Diego, CA, USA). IL-6, TNF-α, and PTHLH levels were measured using mouse IL-6 (583371; Cayman Chemicals, Ann Arbor, MI, USA), TNF-α (500850; Cayman Chemicals), and PTHLH (LS-F15276; LifeSpan Biosciences, Seattle, WA, USA) ELISA kits according to the manufacturer's instructions. The ELISA plates were read using a Synergy HTX Multi-Mode Reader (BioTek Instruments, Winooski, VT, USA).

Free fatty acid, glycerol and TG measurements

Serum levels of triglycerides were measured using the Triglyceride Colorimetric Assay Kit (10010303; Cayman Chemicals). For the detection of both nonesterified fatty acids and free glycerol, 96-well serum/plasma fatty acid and glycerol kit (GFA-1; Zen-Bio, Research Triangle Park, NC, USA) was used.

Hematoxylin and eosin and Oil-Red-O staining

Oil-Red-O staining on differentiated adipocytes and hematoxylin and eosin (H&E) staining on different tissues were performed as previously described (29).

Immunofluorescence staining

For immunofluorescence staining, different tissues [liver, kidney, heart, eWAT, inguinal WAT (iWAT), and BAT] were harvested from 3-mo-old C57BL/6J mice. Slides were deparaffinized in xylol, and antigen retrieval was performed by boiling the slides in water for 30 min. After cooling for 20 min and washing with PBS, the slides were incubated with ZAG primary antibody at a dilution of 1:250 v/v (sc-11243; Santa Cruz

Biotechnology, Dallas, TX, USA) overnight at 4°C. The slides were then washed 3 times with PBS and 0.2% Tween 20 and incubated with AlexaFluor 488 donkey anti-goat (ab150129; Abcam) secondary antibody for 1.5 h at room temperature. The slides were then washed 3 times with PBS and 0.2% Tween 20, air dried for 10 min, and mounted with fluorescence mounting medium (Vectashield H-1200; Vector Laboratories, Burlingame, CA, USA) containing DAPI. The optical images were captured with Keyence BZ-X710 All-in-One Fluorescence Microscope (Osaka, Japan).

Immunoblotting

Whole-cell protein lysates were prepared from cells or tissues using RIPA lysis buffer (89901; Thermo Fisher Scientific) supplemented with Complete Mini Protease Inhibitor Cocktail Tablets (11836153001; Roche, Basel, Switzerland). For Western blot analysis, 50–100 μg of protein was separated on NuPage precast gels (Thermo Fisher Scientific) transferred onto Immobilon-FL membranes (IPFL00010; MilliporeSigma) using an XCell II Blot module (090707-098; Thermo Fisher Scientific), and probed with specific primary antibodies. The following antibodies were used: ZAG (sc-11243; Santa Cruz Biotechnology), steroid receptor coactivator 1 (SRC1; sc-136077; Santa Cruz Biotechnology), PPARγ (MA5-14889; Thermo Fisher Scientific), PPARγ coactivator 1α (PGC1α; sc-13067; Santa Cruz Biotechnology), Ebf2 (AF7006; R&D Systems), p38 MAPK (9212; Cell Signaling Technology, Danvers, MA, USA), phospho-p38 MAPK (4511; Cell Signaling Technology), AP-2 (sc-18661; Santa Cruz Biotechnology), Ucp1 (ab10983; Abcam), Prdm16 (ab106410; Abcam), cell death–inducing DFFA-like effector A (CideA; sc-8732; Santa Cruz Biotechnology), IFN regulatory factor 4 (IRF4; sc-6059; Santa Cruz Biotechnology), iodothyronine deiodinase 2 (Dio2; 26513-1-AP; Proteintech, Rosemont, IL, USA), PTGS2 (ab15191; Abcam), and β-actin (A5441; MilliporeSigma). All antibodies were used at a dilution of 1:1000 (v/v) with the exception of β-actin (1:10,000). The following IRDye-conjugated secondary antibodies were obtained from Li-Cor Biosciences (Lincoln, NE, USA): donkey anti-mouse IRDye800CW (926-32212), donkey anti-rabbit IRDye800CW (926-32213), donkey anti-mouse IRDye680RD (925-68072), donkey anti-rabbit IRDye680RD (925-68073), and donkey anti-goat IRDye680RD (925-68074). Li-Cor Odyssey Classic Imager was used to develop Western blot signals.

Statistical analysis

The quantitative data for the experiments were presented as means ± SD. Statistical analyses were performed using the unpaired Student's *t* test. Values of $P < 0.05$ were considered statistically significant.

RESULTS

ZAG expression is very low in WAT

To evaluate whether ZAG is expressed and secreted by tumors as well as normal tissues or by tumors alone, we analyzed ZAG expression levels in different tissues of wild-type C57BL/6J mice. *ZAG* mRNA transcript levels were very high in the heart, kidney, and liver compared with WAT and BAT (**Fig. 1*A***). At the protein level, however, we detected strong expression of ZAG not only in the heart, kidney, and liver but also in the BAT, whereas ZAG expression was very low in different WATs compared with other tissues (Fig. 1*B*). In addition to Western blot, immunofluorescence staining of ZAG in different tissues revealed strong, predominantly cytoplasmic ZAG staining in BAT as well as liver, kidney, and heart tissues. The staining intensity of ZAG was relatively weaker in WATs compared with other tissues such as BAT and liver (Fig. 1*C–H*). These observations suggest that WATs may not express as much ZAG as some other tissues.

Generation of ZAG expression vectors and ZAG-expressing stable cells

Numerous studies have demonstrated that the circulating levels of ZAG are elevated in various cancers (19–22). To specifically investigate the consequence of increased circulating levels of ZAG on adipose tissue metabolism and energy expenditure, we generated ZAG expression vectors and ZAG-expressing stable cells (Supplemental Fig. 1*A–J*). We generated 2 different ZAG expression plasmids. In the first one, the fluorescent dT reporter was fused with the ZAG protein (ZAG-dT), and in the second plasmid, ZAG and dT sequences were separated by a T2A self-cleaving peptide sequence (Supplemental Fig. 1*A*, *B*). As a result, the dT was not fused with the ZAG protein (Supplemental Fig. 1*C*). Because ZAG is a secretory protein, adding a dT tag could partially inhibit ZAG's secretory function. Therefore, we generated 2 different expression vectors that produced dT-tagged and untagged ZAG. Next, to generate ZAG-expressing stable cell lines, we attempted to identify a cell line with little to no endogenous ZAG expression. To this end, we analyzed ZAG expression levels in different cell lines and found relatively lower endogenous levels of ZAG in MEFs, HEK-293 cells, and C2C12 myoblast cells compared with other cell lines that we tested (Supplemental Fig. 1*D*). Therefore, we generated dT control and ZAG-expressing HEK-293 and MEF stable cell lines (Supplemental Fig. 1*E–J*).

Implantation of ZAG-expressing cells in mice causes lipolysis and induces a brown-like phenotype in WAT

Tumor cells express and secrete various cytokines into the blood stream. One of the major functions of these cytokines is to act on the metabolic organs such as adipose tissues and alter their metabolic functions in such a way that benefits tumor growth. Some of these cytokines not only induce lipolysis in adipose tissues but also promote WAT browning, which accelerates glucose and lipid catabolism, increases body energy expenditure and contributes to cachexia (7, 30). ZAG is one of the cytokines secreted by various cancer cells, and the circulating levels of ZAG are elevated in various cancers. To investigate the consequence of increased circulating levels of ZAG, we implanted 1×10^8 dT control or ZAG-expressing HEK-293 cells subcutaneously in 8–10-wk-old athymic nude mice (**Fig. 2*A***). The implanted cells formed a small mass of tissue (Fig. 2*B*), (dT cell implant 408 ± 17 mg and ZAG cell implant 380 ± 25 mg) constituting ~1.25% of body weight, and histologic analysis of these implants showed similar

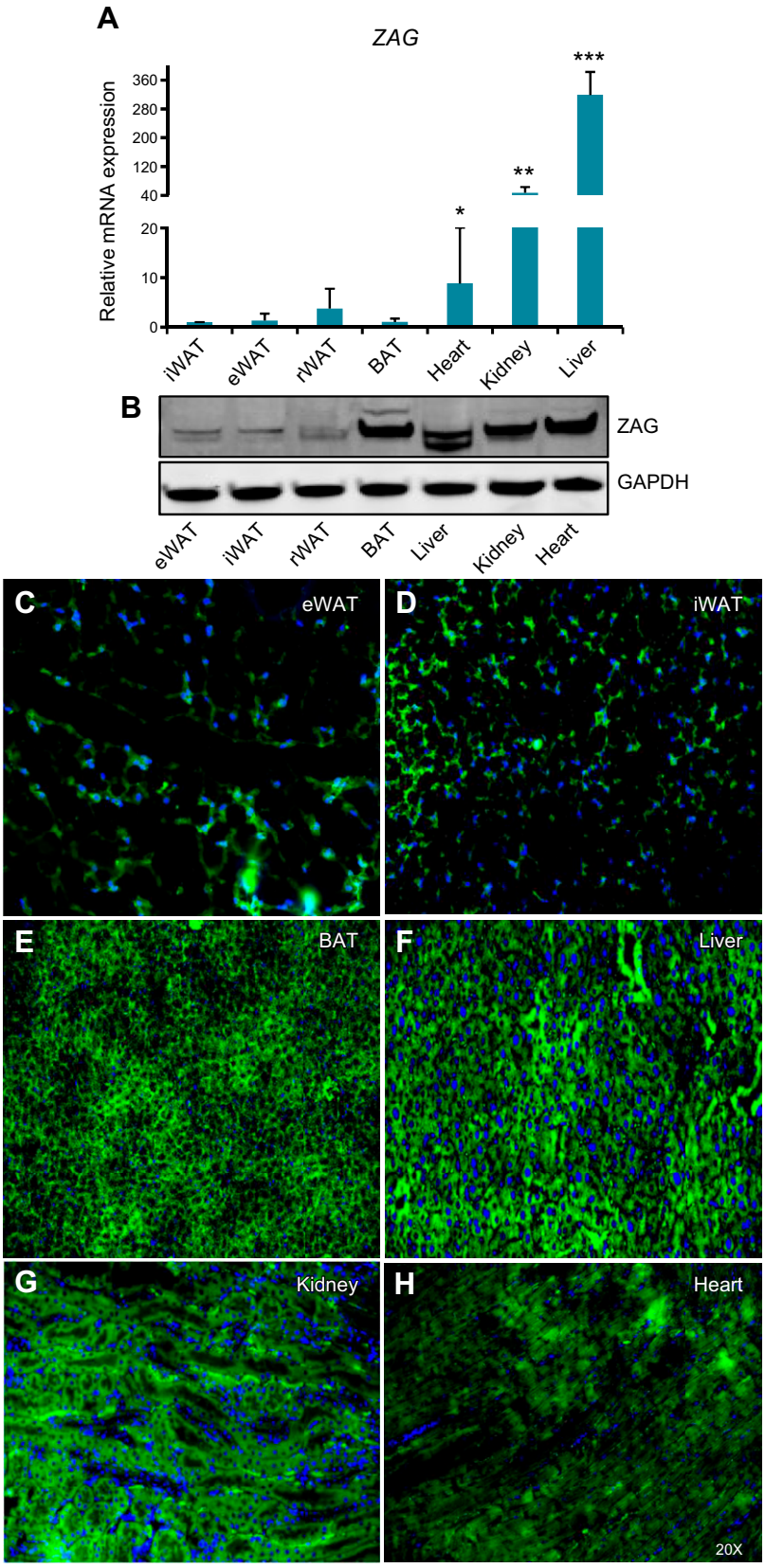

Figure 1. ZAG expression in adult mouse tissues. *A*) *ZAG* mRNA transcript levels in different tissues of 3-mo-old C57BL/6J mice. Compared with its presence in adipose tissues, *ZAG* expression level is significantly higher in heart, kidney, and liver tissues. Data are presented as means ± SD; $n = 4$. $^{*}P < 0.05$, $^{**}P < 0.005$, $^{***}P < 0.0005$. *B*) Expression levels of ZAG protein and GAPDH in different tissues of 3-mo-old C57BL/6J mice. *C–H*) Immunofluorescence staining of ZAG on indicated tissues of 3-mo-old C57BL/6J mice, showing mostly cytoplasmic localization of ZAG in liver, kidney, and BAT. ZAG expression is relatively low in eWAT and iWAT compared with BAT and liver. Original magnification, ×20. rWAT, retroperitoneal WAT.

morphology between dT and ZAG cell implants (Fig. 2*C*). ZAG-expressing cells secreted ZAG (ZAG-dT) as revealed by whole body optical imaging (Fig. 2*A*). In addition, ELISAs revealed ~3-fold higher serum levels of ZAG in mice that received the ZAG cell implant compared with those that received the dT cell implant mice (Fig. 2*D*). Analysis of body weight, eWATs, and BATs 3 wk after implantation revealed no detectable differences between dT, ZAG-dT, or ZAG-expressing cell–implanted mice (Fig. 2*E–H*). Interestingly, however, histologic analysis of

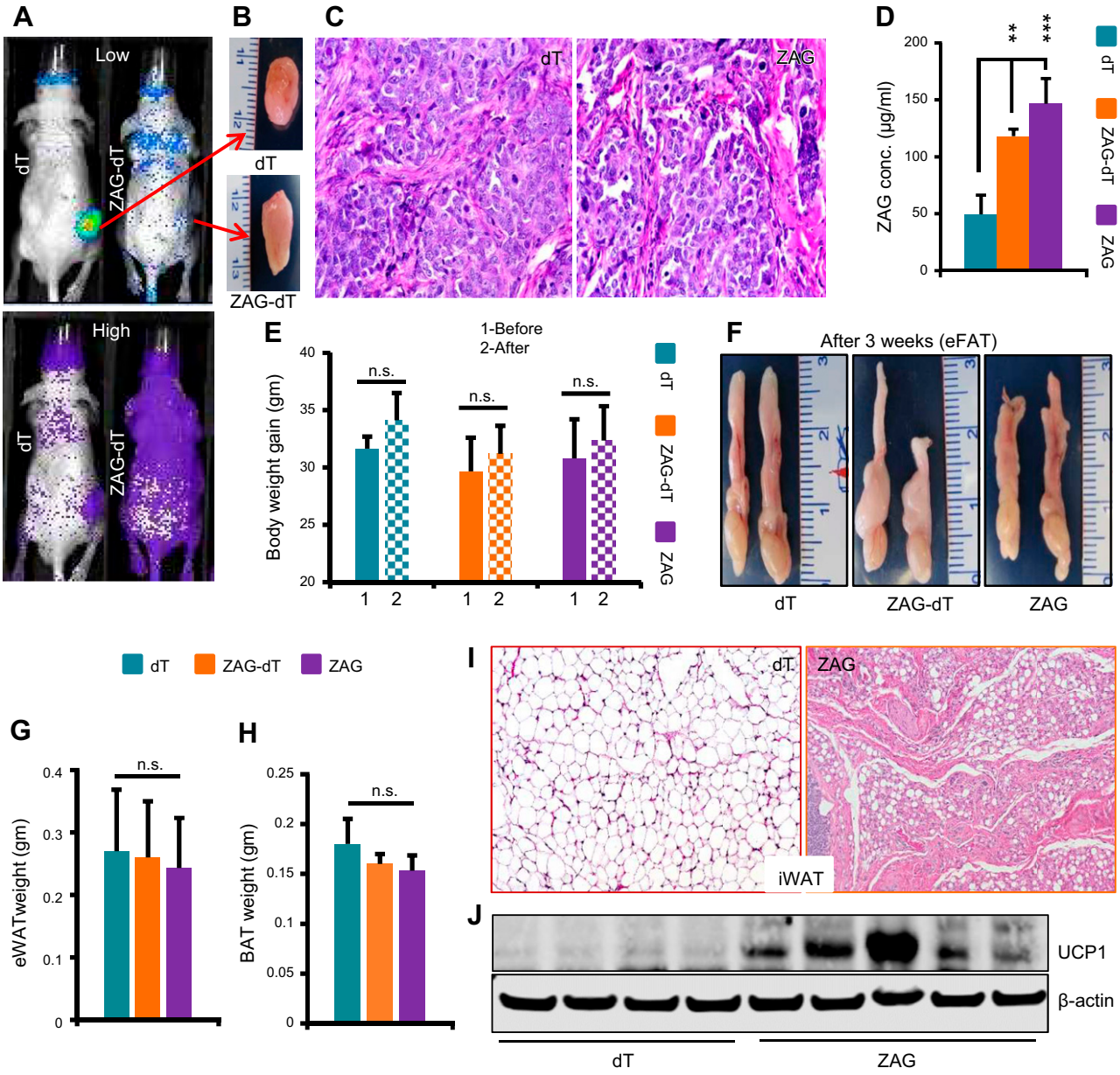

Figure 2. ZAG induces brown-like phenotype in iWAT. *A*) Representative multispectral optical images showing the dT control and ZAG-dT–expressing HEK-293 cell implantation site (red arrows). dT positivity was observed throughout the body of ZAG-dT cell–implanted mice due to circulating ZAG-dT in these mice. *B*) Representative pictures showing a small tissue mass that was formed by the HEK-293 cells 6 wk after implantation. *C*) Representative H&E-stained sections of dT- and ZAG-expressing HEK-293 cell implants harvested from nude mice 6 wk after implantation. *D*) Serum levels of ZAG in athymic nude mice 3 wk after subcutaneous implantation of dT, ZAG-dT, and ZAG HEK-293 cells. Data are presented as means ± SD; $n = 5$. $^{**}P < 0.005$, $^{***}P < 0.0005$. *E*) Body weight of dT, ZAG-dT, and ZAG cell–implanted mice before and 3 wk after implantation. Data are presented as means ± SD; $n = 5$. *F*) Representative pictures of eWAT pads in athymic nude mice 3 wk after implantation of dT, ZAG-dT, and ZAG HEK-293 cells. *G*, *H*) Average weight of eWAT pads (*G*) and BAT (*H*) in mice 3 wk after implantation of dT-, ZAG-dT– or ZAG-expressing HEK-293 cells. Data are presented as means ± SD; $n = 5$. *I*) Representative H&E-stained iWAT of athymic nude mice 3 wk after implantation of dT- or ZAG-expressing HEK-293 cells. *J*) Expression level of Ucp1 in the iWAT of dT- or ZAG-expressing cell–implanted mice. N.s., not significant.

iWAT revealed a brown fat-like morphology (Fig. 2*I*) and expression of UCP1 in ZAG cell–implanted mice (Fig. 2*J*). These observations suggested that higher circulating levels of ZAG might have caused browning in iWAT and might produce a significant visible effect on other adipose tissues at later time-points. Therefore, we analyzed mice 6 wk after implantation and observed significant adipose tissue atrophy in mice implanted with ZAG-dT– or ZAG-expressing cells compared with dT cell–implanted mice (**Fig. 3*A*–*C***). The body weight of dT cell–implanted mice increased by ~4 g between the day of implantation (d 1) to the day of euthanization (6 wk) (Fig. 3*D*). This was expected because we implanted cells in 8–10-wk-old mice that were in an active growth phase. Conversely, ZAG cell–implanted mice did not gain any body weight in that 6-wk period (Fig. 3*D*). Due to WAT atrophy, the weight of

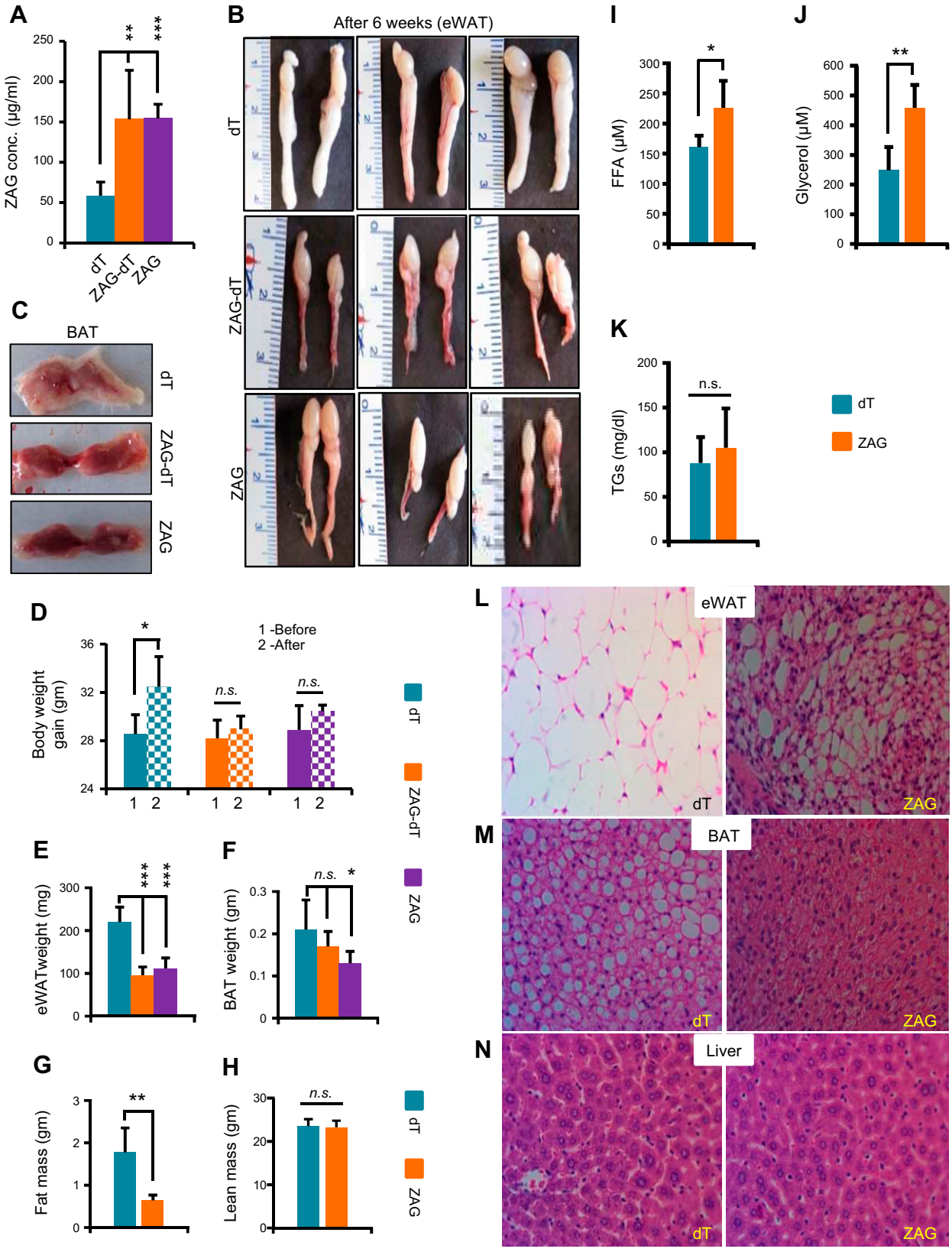

Figure 3. ZAG induces atrophy and a brown-like phenotype in eWAT. *A*) Serum levels of ZAG in athymic nude mice 6 wk after subcutaneous implantation of dT, ZAG-dT, and ZAG HEK-293 cells. Data are presented as means ± SD; $n = 6$. $^{**}P < 0.005$, $^{***}P < 0.0005$. *B*, *C*) Representative pictures of eWAT pads (*B*) and interscapular BAT (*C*) in athymic nude mice 6 wk after implantation of dT-, ZAG-dT–, or ZAG-expressing HEK-293 cells. *D*) Body weight of dT, ZAG-dT and ZAG cell–implanted mice before and 6 wk after implantation. Data are presented as means ± SD; $n = 5$. $^{*}P < 0.05$. *E*, *F*) Average weight of eWAT pads (*E*) and BAT (*F*) in mice 6 wk after implantation of dT, ZAG-dT– or ZAG-expressing HEK-293 cells. Data are presented as means ± SD; $n = 6$.

(*continued on next page*)

eWAT as well as total body fat mass were significantly reduced in ZAG cell–implanted mice, but lean mass was unaffected (Fig. 3*E–H*). The circulating levels of free fatty acid and glycerol were significantly higher in ZAG cell–implanted mice compared with dT cell–implanted mice (Fig. 3*I–K*). These observations suggest that ZAG caused massive lipolysis in WAT, resulting in the depletion of lipids from WAT. Because both ZAG-dT and ZAG cell–implanted mice showed similar WAT atrophy phenotype we utilized dT control and ZAG cell–implanted mice for further analysis. iWAT had completely disappeared in ZAG cell–implanted mice 6 wk after implantation; therefore, we were able to analyze only eWAT. Remarkably, histologic analysis revealed a BAT-like morphology in the eWAT of ZAG cell–implanted mice compared with control mice (Fig. 3*L*). Further analysis revealed reduced lipid accumulation in the BAT and liver of ZAG cell–implanted mice compared with dT cell–implanted mice (Fig. 3*M, N*).

Because tumor secretory factors IL-6 and TNF-α are known to cause adipose tissue atrophy, we asked whether ZAG directly induced adipose tissue atrophy or indirectly elevated IL-6 and TNF-α levels, which in turn caused adipose tissue atrophy and the brown-like phenotype within WAT. Analysis of IL-6 and TNF-α in control and ZAG-expressing cell–implanted mice revealed no significant differences in the circulating levels of IL-6 and TNF-α, indicating that ZAG does not induce these 2 cytokines (Supplemental Fig. 2*A*, *B*). We also did not detect any significant difference in the serum levels of PTHrP, a tumor secretory factor known to induce WAT browning, between dT and ZAG cell–implanted mice (Supplemental Fig. 2*C*) (30). Next, we asked whether ZAG induced atrophy predominantly in the adipose tissues or in other organs as well. Histologic analysis of the kidney, heart, and testes revealed no detectable changes between dT- and ZAG-expressing cell–implanted mice (Supplemental Fig. 2*D–F*), suggesting that ZAG largely acted on the adipose tissues. We also attempted to perform similar cell implantation experiments with dT control or ZAG-expressing immortalized MEFs (1×10^8) in athymic nude mice. Although the implanted MEFs survived in nude mice, after 3 and 6 wk the circulating levels of ZAG were only slightly elevated in ZAG cell–implanted mice compared with dT cell–implanted mice. As a result, these mice did not show any detectable phenotype (data not included). This occurred possibly because the expression level of ZAG in stable MEF cells was significantly lower than that of stable HEK-293 cells (Supplemental Fig. 1*J*). Taken together, our results suggest that higher circulating levels of ZAG not only cause lipolysis in WAT but also induce a brown-like phenotype in WAT.

ZAG strongly induces the expression of beige, mitochondrial, and thermogenic genes in WAT

WAT browning is known to occur predominantly in iWAT followed by eWAT in response to certain stimuli such as β3-AR agonists (17, 31). To investigate whether ZAG induced browning in WAT, we analyzed the expression of beige, thermogenic, and mitochondrial genes, and detected a strong up-regulation of these genes in the eWAT of ZAG-cell- implanted mice compared with dT cell–implanted mice (**Fig. 4*A–C***). In ZAG cell–implanted mice, iWAT was reduced after 3 wk and we were unable to extract sufficient amounts of RNA or protein for more extensive analysis. iWAT had completely disappeared in ZAG cell–implanted mice 6 wk after implantation. Therefore, we mainly utilized eWAT for further molecular analysis. Brown-like adipocytes within WAT can be generated in response to prolonged cold exposure or PPARγ and β3-AR agonists. Stimulation of β3-AR in turn activates PKA, which ultimately induces or stabilizes Prdm16. By inducing the expression of PPARα, CEBPβ, PPARγ, and PGC1α, Prdm16 promotes brown-like differentiation (15, 17, 31, 32). Because activation of β3-AR signaling is one of the earlier events that occur during the differentiation of progenitors into brown-like adipocytes, we asked whether ZAG activated the β3-AR/PKA signaling pathway. Analysis of PKA activation by measuring the phosphorylation levels of PKA substrates revealed significantly higher PKA substrate activation in the eWAT of ZAG cell–implanted mice compared with dT cell–implanted mice (Fig. 4*D*). Consequently, we also detected strong up-regulation of brown adipocyte thermogenic genes such as Ebf2, Prdm16, PGC1α, SRC1, CideA, IRF4, and Ucp1 at the protein level in the eWAT of ZAG cell–implanted mice compared with dT cell–implanted mice (Fig. 4*D*). β3-AR activation also induces PTGS2, a rate limiting enzyme in prostaglandin synthesis, which is known to promote WAT browning (33). Because higher circulating levels of ZAG appear to activate the β3-AR pathway, we also measured and detected elevated levels of PTGS2 (Fig. 4*E*) and increased PTGS2 enzymatic activity (Fig. 4*F*) in the eWAT of ZAG cell–implanted mice compared with dT cell–implanted mice. Collectively, these data suggest that elevated circulating levels of ZAG stimulate the β3-AR pathway, induce thermogenic gene expression, and cause WAT browning.

ZAG promotes brown adipocyte differentiation in white adipose progenitors

WAT consists of not only mature adipocytes filled with triglycerides but also an SVF in which the preadipocytes or white adipocyte progenitors reside (34). In response to

$^*P < 0.05$, $^{***}P < 0.0005$. *G*, *H*) Total body fat mass (*G*) and lean mass (*H*) of dT and ZAG cell–implanted mice 6 wk after implantation measured by LF90II BCA-Analyzer. Data are presented as means ± SD; $n = 5$; $^{**}P < 0.005$. *I–K*) Serum levels of free fatty acid (*I*), glycerol (*J*), and triglycerides (*K*) in dT and ZAG cell–implanted mice 6 wk after implantation. Data are presented as means ± SD; $n = 5$. $^*P < 0.05$, $^{**}P < 0.005$. *L–N*) Representative H&E stained eWAT (*L*), BAT (*M*), and liver (*N*) sections of athymic nude mice 6 wk after implantation of dT- or ZAG-expressing HEK-293 cells. N.s., not significant.

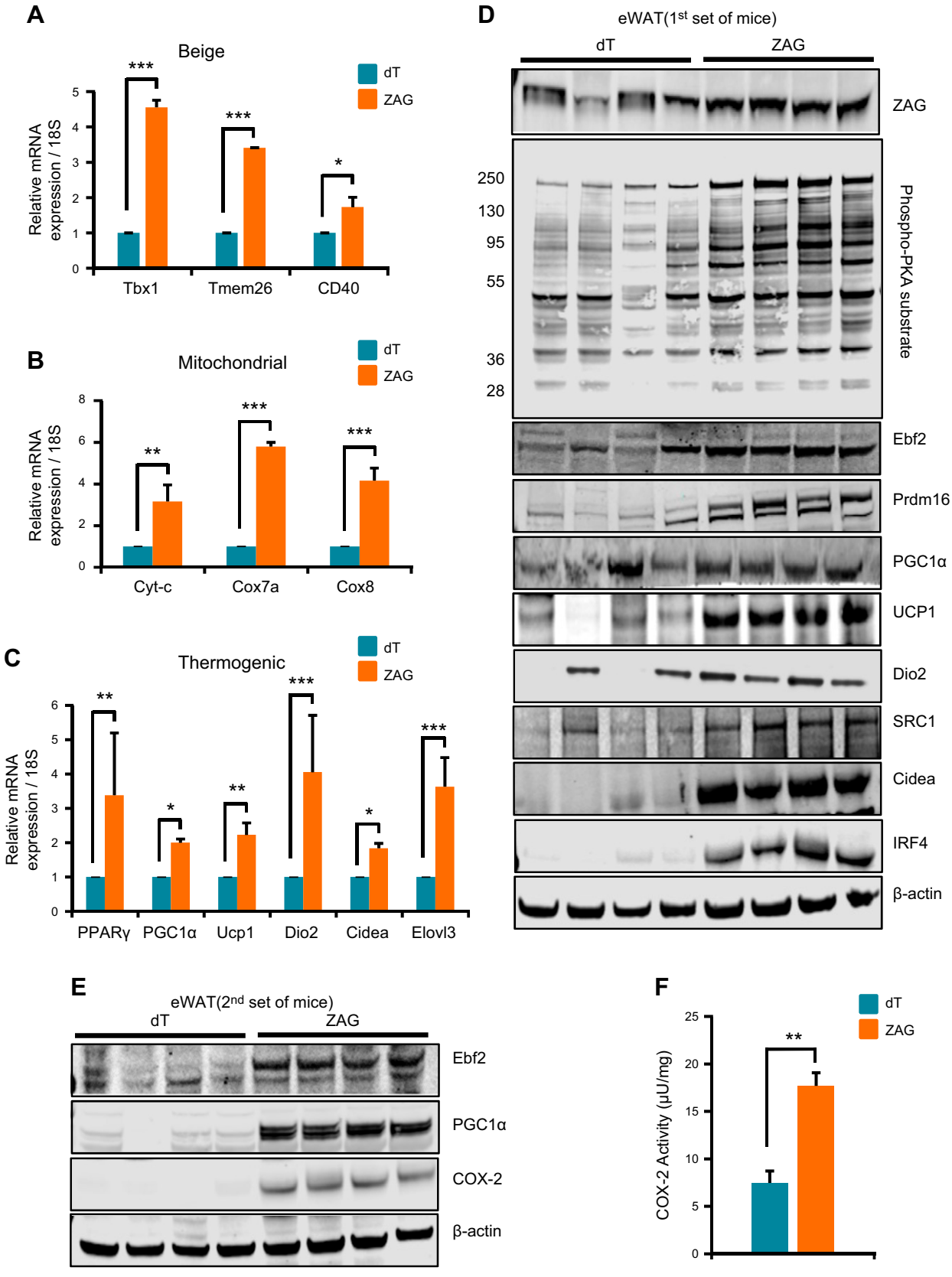

Figure 4. ZAG induces thermogenic gene expression in the eWAT. *A–C*) Relative mRNA transcript levels of beige, mitochondrial, and thermogenic genes in the eWAT of dT- or ZAG-expressing cell–implanted mice. All the qPCR data are presented as means ± SD; $n = 5$. $^*P < 0.05$, $^{**}P < 0.005$, $^{***}P < 0.0005$. *D*) Expression levels of indicated proteins in the eWAT of dT- or ZAG-expressing cell–implanted mice (first set of mice). *E*) Expression levels of Ebf2, PGC1α, and PTGS2 in the eWAT of dT- and ZAG-expressing

(*continued on next page*)

thermogenic stimuli such as prolonged cold exposure or PPARγ and β3-agonist treatments, white adipocyte progenitors differentiate into brown-like (beige or brite) cells resulting in WAT browning (15, 17, 31). Because ZAG cell–implanted mice, which exhibited ~3-fold higher circulating levels of ZAG, showed a brown-like phenotype in WAT, we wondered whether ZAG, in addition to depleting lipid from the mature white adipocytes, was also stimulating white adipocyte progenitors to differentiate into brown-like cells. To investigate this possibility, we harvested the SVF from wild-type C57BL/6J mice WATs and cultured white adipose progenitors as previously described (13, 35). We detected a robust increase in the differentiation of white adipocyte progenitors into brown adipocytes when the differentiation medium was supplemented with ZAG recombinant protein (1 μg/ml) as revealed by enhanced expression of the adipocyte differentiation marker adipocyte protein 2 (aP2) and Oil-Red-O staining (**Fig. 5*A–D***). At the molecular level, adipose progenitors differentiated in the presence of ZAG protein displayed increased expression of beige (CD40, CD137), mitochondrial (Cox7a, Cox8b), and thermogenic (Ebf2, Prdm16, PPARγ, PGC1α, SRC1, Dio2, CideA, and Ucp1) genes on differentiated cells from d 4 and d 8 compared with vehicle-treated cells (Fig. 5*D, E*). These results indicate that ZAG promoted differentiation of white adipose progenitors into brown-like cells by stimulating the expression of PPARγ, Ebf2, Prdm16, and PGC1α. When we treated cells with higher concentration of ZAG recombinant protein (2.5 μg/ml), however, we detected impaired proliferation and increased death of progenitor cells, suggesting that higher levels of ZAG could be toxic to the cells.

ZAG stimulates brown-like differentiation in MEFs

To further investigate whether ZAG did indeed stimulate brown-like differentiation in progenitor cells, we utilized dT- and ZAG-expressing MEFs as an alternative model. MEFs are unprogrammed cells that share several characteristics with mesenchymal stem cells and can differentiate into a number of mesenchymal lineages (36). MEFs can also be induced to differentiate into brown-like adipocytes (37). Thus, we attempted to generate primary MEFs with stable ZAG expression. These cells showed impaired proliferation and increased cell death in response to ZAG expression followed by drug selection, however, indicating that primary MEFs are sensitive to higher levels of ZAG expression. Thus, we utilized immortalized MEFs. Unlike primary MEFs, immortalized MEFs do not efficiently differentiate into adipocytes unless either PPARγ or CCAAT enhancer binding protein (CEBP) α is expressed (38). Therefore, we asked if ZAG induces differentiation in immortalized MEFs by inducing the expression of PPARγ, the master regulator of adipocyte differentiation (39, 40). As expected, we detected very little adipocyte differentiation in the control immortalized MEFs; however, ZAG-expressing immortalized MEFs showed increased differentiated as revealed by enhanced expression of aP2 and Oil-Red-O staining (**Fig. 6*A–I, K***). At the molecular level, ZAG-expressing MEFs displayed stronger induction of PPARγ (Fig. 6*J, K*) and increased expression of beige, mitochondrial, and thermogenic genes in cells that differentiated on d 2 and 4 than did dT-MEFs (Fig. 6*I, J*). At the protein level, ZAG expression was strongly induced in the course of differentiation (Fig. 6*K*), and ZAG-expressing MEFs displayed strong expression of aP2, PPARγ, Ebf2, Prdm16, PGC1α, SRC1, Dio2, and Ucp1 during differentiation, whereas dT-MEFs did not show expression of these proteins because they had not differentiated (Fig. 6*K*). Together, these results indicate that ZAG promoted differentiation of MEFs into brown-like cells by stimulating the expression of PPARγ, Ebf2, Prdm16, and PGC1α.

ZAG induces Prdm16 expression by promoting Ebf2/PPARγ recruitment to the *Prdm16* promoter

In the adipose progenitors, Ebf2 induces *Prdm16* expression by recruiting PPARγ to the *Prdm16* promoter. Once induced, Prdm16 promotes expression of PPARα, CEBPβ, PPARγ, and PGC1α, thereby determining brown adipocyte cell fate (11–13, 15, 17, 32). In the eWAT of ZAG cell–implanted mice, and in differentiating adipose progenitors and differentiating MEFs, we detected increased expression of Prdm16 (Figs. 4*D*, 5*E*, and 6*J, K*). Therefore, we asked whether ZAG induced *Prdm16* expression *via* Ebf2/PPARγ, both of which were strongly up-regulated in response to ZAG (Figs. 4*C*, 5*E*, and 6*J, K*). To investigate this possibility, we coexpressed a *Prdm16* promoter–driven luciferase reporter vector along with *Ebf2*, *PPARγ*, and *RXRα* (*retinoic acid receptor α*) in the presence or absence of a *ZAG* expression vector. In the absence of both PPARγ and Ebf2, ZAG expression alone did not result in any *Prdm16* reporter activity (**Fig. 7*A***). We observed induction of *Prdm16* reporter activity in the presence of PPARγ alone, which was slightly enhanced when coexpressed with ZAG. In contrast, increased induction of *Prdm16* was observed when both Ebf2 and PPARγ were expressed, and was strongly enhanced when ZAG was coexpressed (Fig. 7*A*), indicating that ZAG induces *Prdm16* expression *via* Ebf2/PPARγ. It was demonstrated that Ebf2 recruits PPARγ to the *Prdm16* promoter after binding to the *Prdm16* promoter, thus driving *Prdm16*

cell–implanted mice (second set of mice). In the first set of control mice, 1 or 2 mice exhibited high background levels of Ebf2 and PGC1α (*D*); therefore, we further confirmed their differential expression by repeating the experiment (second set). *F*) PTGS2 enzymatic activity in the eWAT lysates of dT- and ZAG-expressing cell–implanted mice. Data are presented as means ± SD; $n = 4$. $^{**}P < 0.005$. PTGS2 expression and activity assays were performed using tissue lysates from second set because we did not have sufficient tissue lysates available from the first set. Tissues were collected 6 wk after the cell implantations.

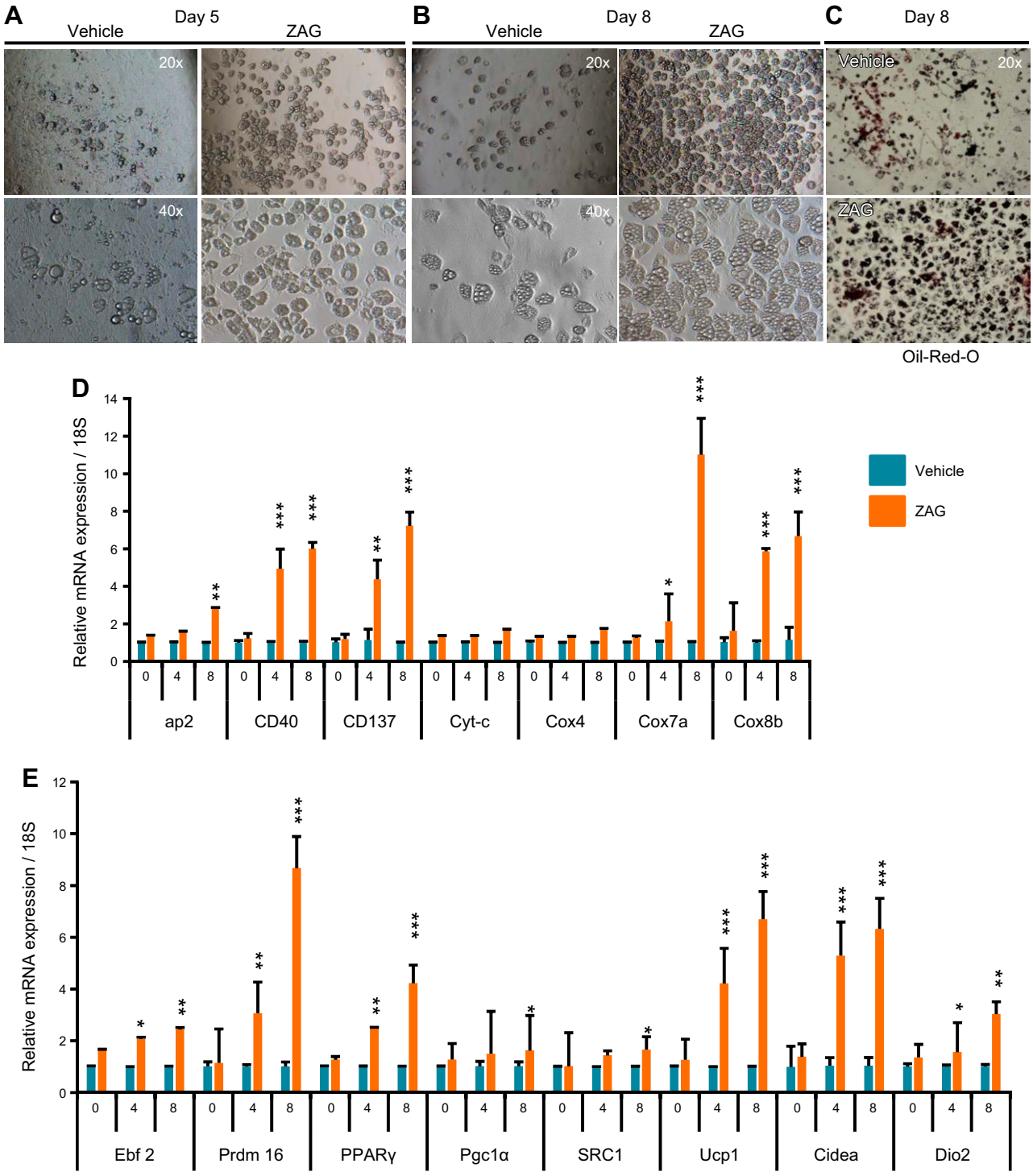

Figure 5. ZAG stimulates brown adipogenesis in white adipose progenitors. *A*, *B*) Representative bright-field images of white adipose progenitor cells that differentiated on d 5 and 8, showing more adipocyte morphology in ZAG recombinant protein treated cells. *C*) Oil-Red-O staining pictures of vehicle or ZAG protein–treated white adipose progenitor cells that differentiated on d 8. *D*, *E*) Relative mRNA transcript levels of beige, mitochondrial, and thermogenic genes in adipose progenitors that differentiated on d 0, 4, and 8 and were treated with vehicle (PBS) or ZAG recombinant protein (1 μg/ml medium). Data are presented as means ± SD; $n = 3$. *$P < 0.05$, **$P < 0.005$, ***$P < 0.0005$.

expression (13). Therefore, we asked if ZAG promoted Ebf2-mediated recruitment of PPARγ to the *Prdm16* promoter. ChIP-qPCR assays on control and ZAG-expressing MEFs that differentiated on d 5 revealed increased binding of both Ebf2 and PPARγ to the *Prdm16* promoter region in ZAG-expressing MEFs compared with dT-expressing MEFs (Fig. 7*B*, *C*). These observations together indicate that ZAG stimulated Prdm16 expression by inducing the expression of Ebf2 and PPARγ and promoting their recruitment to the *Prdm16* promoter.

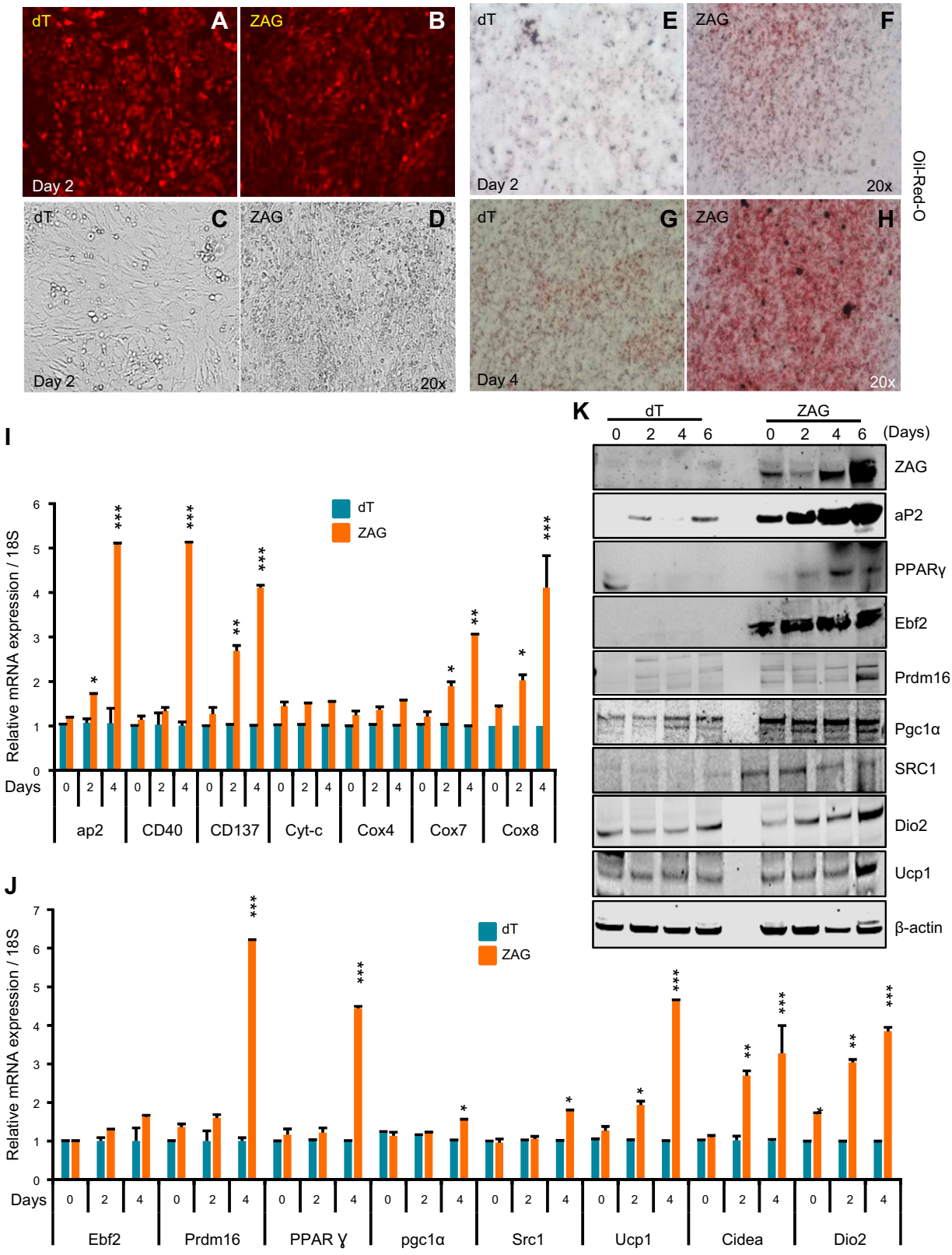

Figure 6. ZAG promotes brown adipogenesis in MEFs. *A*, *B*) Representative images showing the expression of dT or ZAG (untagged dT) in MEFs that differentiated on d 2. *C*, *D*) Bright-field images showing increased round adipocyte morphology in ZAG-expressing MEFs that differentiated on d 2 compared with dT-expressing MEFs that differentiated at the same time. *E–H*) Oil-Red-O staining pictures of ZAG-expressing MEFs that differentiated on d 2 and d 4 compared with dT-expressing MEFs. *I*, *J*) Relative mRNA transcript levels of beige, mitochondrial, and thermogenic genes in ZAG-expressing MEFs that differentiated on d 0, 2, and 4 compared with dT-expressing MEFs. Data are presented as means ± SD; $n = 3$. $^{*}P < 0.05$, $^{**}P < 0.005$, $^{***}P < 0.0005$. *K*) Western blots showing the expression levels of ZAG, aP2, and different thermogenic proteins in differentiating dT- and ZAG-expressing MEFs at the indicated time points after inducing brown adipogenesis.

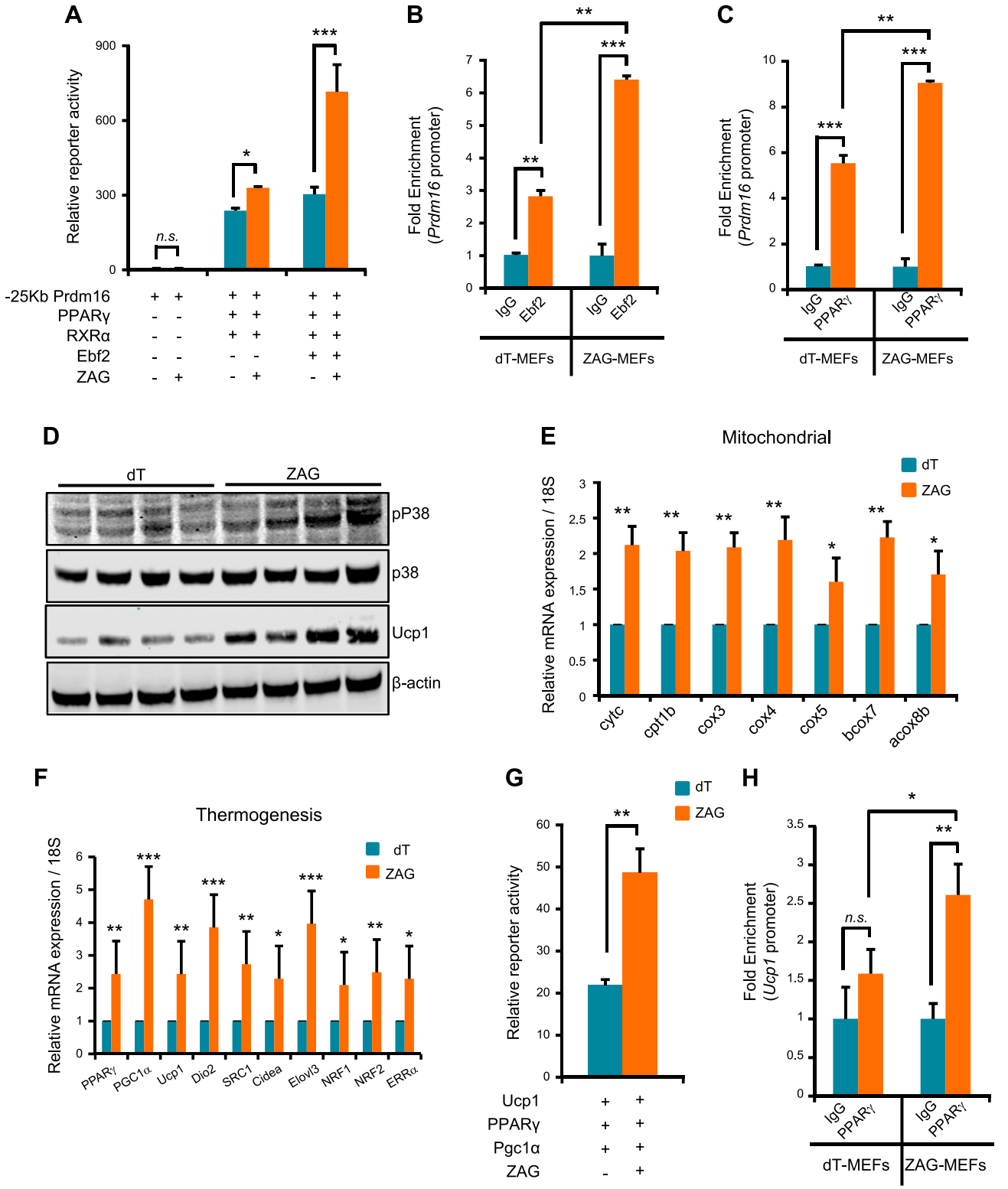

Figure 7. ZAG increases PPARγ and Ebf2 recruitment to Prdm16 promoter. *A*) Relative reporter activity of *Prdm16* promoter–driven luciferase activity in the presence of PPARγ, RXRα, and Ebf2, and in the presence or absence of ZAG expression. Data are presented as means ± SD; $n = 3$. $^*P < 0.05$, $^{***}P < 0.0005$. ZAG strongly enhanced *Prdm16* promoter–driven luciferase activity when Ebf2 was present. *B, C*) ChIP-qPCR analysis of Ebf2 binding to the *Prdm16* promoter (*B*), and PPARγ binding to the *Prdm16* promoter (*C*) in dT and ZAG MEFs that differentiated on d 5 after normalizing to 18S binding. Data are presented as means ± SD; $n = 2$. $^{**}P < 0.005$, $^{***}P < 0.0005$. *D*) Western blots showing the expression levels of indicated proteins in the BAT of dT- and ZAG-expressing cell–implanted mice. *E, F*) Relative mRNA transcript levels of mitochondrial (*E*) and thermogenic (*F*) genes in the BAT of dT or ZAG-expressing cell–implanted mice. BAT tissues were analyzed 6 wk after cell implantation in athymic nude mice. Data are presented as means ± SD; $n = 5$. $^*P < 0.05$, $^{**}P < 0.005$, $^{***}P < 0.0005$. *G*) Relative

(*continued on next page*)

ZAG activates thermogenesis in interscapular BAT

Our data, so far, suggest that ZAG played a predominant role in inducing brown-like differentiation in WAT by regulating the Ebf2/PPARγ/Prdm16 pathway. Next, we asked whether increased circulating levels of ZAG only caused browning in WAT or if it also activated thermogenesis in the existing interscapular BAT. In response to thermogenic stimuli, β3-AR and PKA phosphorylate and activates p38 MAPK, which in turn activates PGC1α in the BAT. Upon binding to PPARγ, PGC1α regulates the expression of the majority of the thermogenic genes including Ucp1 (17). We detected increased activation of p38 MAPK in the BAT of ZAG cell–implanted mice compared with dT cell–implanted mice (Fig. 7*D*). Consequently, we detected strong induction of the majority of the thermogenic genes including Ucp1 in the BAT of ZAG cell–implanted mice compared with dT cell–implanted mice (Fig. 7*D–F*). Next, we asked whether ZAG induced *Ucp1* expression by promoting PPARγ and PGC1α binding to the *Ucp1* promoter. To this end, we coexpressed a *Ucp1* promoter–driven luciferase reporter vector along with *PPARγ* and *PGC1α* in the presence or absence of the *ZAG* expression vector. ZAG expression significantly increased the *Ucp1* reporter activity (Fig. 7*G*). To further confirm that ZAG indeed promoted PPARγ and PGC1α recruitment to the *Ucp1* promoter, we performed ChIP-qPCR assays on MEFs that differentiated on d 5, which revealed increased binding of PPARγ to the *Ucp1* promoter region in ZAG-expressing MEFs compared with dT-expressing MEFs (Fig. 7*H*). Collectively, these data suggest that ZAG stimulates Ucp1 expression in BAT by promoting the recruitment of PPARγ and PGC1α to the *Ucp1* promoter.

DISCUSSION

The majority of tumors produce and discharge large numbers of cytokines into the circulation. These cytokines target various organs and alter their cellular or metabolic functions. Although many cytokines function independently, they often work in coordination with other cytokines to produce a more potent effect (41). Therefore, understanding the individual contribution of a specific tumor secretory factor to the development of any of the symptoms of cachexia is relatively difficult. It requires an animal model in which only the cytokine of interest needs to be secreted continuously from an implant or tissue. This facilitates investigation into its role in metabolic alteration, WAT browning, and cachexia. Some previous studies attempted to understand the effects of individual cytokines by administering purified recombinant proteins in animal models (42, 43). However, one of the drawbacks of this approach is that some cytokines are short lived and produce a strong acute effect immediately after administration that gradually wears off. This does not perfectly mimic tumor-induced cachexia, in which a tumor continuously produces and releases various cytokines into the blood stream. To mimic tumor-induced cachexia and investigate the specific functions of ZAG in adipose tissue–specific metabolic alterations, we utilized an *in vivo* cell implantation model. Our model closely mimics secretion of ZAG from a tumor, allowing us to explore the role of ZAG in the development of some symptoms of cachexia.

ZAG has been known as a lipid mobilizing factor that induces lipolysis in white adipocytes (23, 24). We observed relatively low expression of ZAG in WAT compared with other tissues. ZAG is highly expressed in numerous cancers, and ZAG levels are elevated in the serum of cancer patients (19–22). This raises an important question: What happens when the circulating levels of ZAG are elevated? We detected extensive lipolysis and lipid depletion in the WATs of ZAG cell–implanted mice, where ZAG levels are ~3-fold higher. Interestingly, although we found higher circulating levels of ZAG, lipid depletion and WAT atrophy did not happen quickly but rather occurred slowly; extensive WAT atrophy was not detected until 6 wk after ZAG cell implantation. This specifies that under *in vivo* conditions, ZAG-induced lipolysis and lipid depletion were relatively slow processes. ZAG stimulates lipolysis in adipocytes *via* activation of β3-AR and activation of the cAMP pathway (27). Stimulation of β3-AR in turn activates PKA, which phosphorylates hormone-sensitive lipase and increases adipocyte lipolysis (44). In this context, an important question arises: If ZAG has the ability to stimulate β3-AR, does ZAG promote WAT browning? This question arises mainly because activation of the β3-AR pathway not only stimulates lipolysis in white adipocytes but also stimulates thermogenesis in mature brown adipocytes, and chronic β3-AR activation causes WAT browning (15–17, 45). Consistent with this idea, we detected a brown-like phenotype in the WATs of mice when the circulating levels of ZAG were persistently elevated. The expression of beige, mitochondrial, and thermogenic genes such as Ebf2, Prdm16, PGC1α, Ucp1, SRC1, and IRF4 were strongly induced in WAT when the circulating ZAG levels were elevated. Moreover, PTGS2, a rate-limiting enzyme in prostaglandin synthesis that functions downstream of β3-AR and promotes WAT browning (33), was also strongly induced in WAT in response to ZAG. Overall, our observations suggest that ZAG activated the β3-AR pathway and induced robust browning in WAT. In response to chronic cold exposure, which stimulates β3-AR, or treatment with β3-AR or PPARγ agonists, *Ucp1*-expressing beige adipocytes developed within WAT. These stimuli induced white adipose progenitors in WAT to differentiate into brown-like adipocytes (15, 17, 31, 46, 47). Interestingly, stimulation of white adipose progenitors with ZAG recombinant protein or expression

reporter activity of *Ucp1* promoter–driven luciferase activity in the presence of PPARγ and PGC1α (independent of each other), and in the presence or absence of ZAG expression. Data are presented as means ± SD, $n = 3$. $^{**}P < 0.005$. *H*) ChIP-qPCR analysis of PPARγ binding to the *Ucp1* promoter in dT and ZAG MEFs that differentiated on d 5 after normalizing to 18S binding. Data are presented as means ± SD; $n = 2$. $^{*}P < 0.05$, $^{**}P < 0.005$. N.s., not significant.

of ZAG in immortalized MEFs significantly enhanced brown-like differentiation *in vitro*. Although differentiation of white adipose progenitors into beige adipocytes is the main contributor to WAT browning, we cannot completely exclude the possibility that a small fraction of mature white adipocytes might also have transdifferentiated into brown-like cells in response to ZAG, which drained lipid from the mature adipocytes.

Beige adipocytes are mainly derived from adipose progenitor or precursor cells (10), in which induction of Prdm16 transcriptionally activates several factors such as PPARα, PPARγ, and PGC1α to promote beige adipocyte differentiation (12, 14). Ebf2 and PPARγ function upstream to Prdm16; Ebf2 recruits PPARγ to the *Prdm16* promoter, which in turn induces *Prdm16* expression (11–13). Forced expression of *Prdm16* or *Ebf2* is sufficient to drive white adipose precursors into brown-like Ucp1-expressing cells *in vitro* and *in vivo* (11, 14–16). Prolonged cold exposure and PPARγ or β3-AR agonist treatments that promote WAT browning also activate or stabilize Prdm16 (16, 17, 31). Collectively, these studies demonstrate that the Ebf2/PPARγ/Prdm16 pathway plays a central role in the differentiation of adipose progenitors into brown-like cells. In response to increased circulating levels of ZAG, we found enhanced expression of Prdm16 in WAT and in differentiating adipose progenitors and MEFs. At the molecular level, forced expression of ZAG increased expression of PPARγ and Ebf2 and also recruited them to the *Prdm16* promoter, suggesting that ZAG activates the Ebf2/PPARγ/Prdm16 pathway to drive white adipose progenitors toward brown-like cells. Therefore, ZAG appears to function similarly to a β3-AR agonist, and the observed WAT browning phenomenon in ZAG cell–implanted mice could be due to ZAG's ability to force white adipose progenitors to differentiate into brown-like cells. A previous study showed that when the primary adipocytes isolated from BAT and WAT were incubated with purified ZAG protein, it induced *Ucp1* mRNA in brown but not in white adipocytes (48). In this study, they treated cells with ZAG protein for 24 h. In our *in vivo* model, the circulating levels of ZAG were persistently higher for 6 wk, and we detected a brown-like phenotype in iWAT and eWAT after 3 and 6 wk respectively, suggesting that ZAG-induced browning or induction of thermogenic genes are long-term rather than short-term results.

The β3-AR/PKA/p38 MAPK pathway is known to phosphorylate and activate PGC1α (17). PGC1α is the master transcriptional coactivator that is involved in the activation of thermogenesis in BAT in response to cold or β3-AR stimuli (49–51). In the BAT of ZAG cell–implanted mice, we detected increased phosphorylation and activation of p38 MAPK and increased recruitment of PPARγ to the downstream target genes such as *Ucp1* promoter, which resulted in enhanced expression of Ucp1 and other thermogenic genes. There are contradicting reports on the induction of *Ucp1* and activation of thermogenesis in BAT in response to treatment with ZAG recombinant protein. A few studies demonstrated that purified ZAG protein induced *Ucp1* expression in primary brown adipocytes and administration of ZAG in mice caused up-regulation of *Ucp1* mRNA and protein in BAT (27, 48, 52); however, another recent study showed no induction of *Ucp1* or activation of thermogenesis in response to ZAG administration (53). These discrepancies could result from differences in the amount of ZAG protein administered, length of treatment, and the specific mouse strains used. In our model, which closely mimics secretion of ZAG from a tumor, we observed not only strong induction of thermogenic genes, including Ucp1, in BAT but also robust browning in WAT in response to ZAG.

Our observations raise another important question: Do secretory factors or cytokines have the ability to induce WAT browning, which is known to occur mainly in response to chronic cold exposure or prolonged β3-AR agonist treatments? It was recently demonstrated that circulating levels of IL-6 are increased in cachectic mice and humans (7, 54) and promote WAT browning in mice, suggesting that IL-6 is one of the mediators of WAT browning (7). It was also demonstrated that tumor-derived PTHLH causes WAT browning in the Lewis lung carcinoma model of cancer cachexia (30). In our model, higher circulating levels of ZAG did not induce IL-6, TNF-α, or PTHLH production, suggesting that ZAG does not require IL-6 or PTHLH to induce WAT browning. We performed implantation experiments on athymic nude mice, however, which may not produce elevated levels of IL-6 and TNF-α in response to external stimuli. Nevertheless, ZAG was able to induce WAT browning regardless of whether IL-6 and TNF-α were stimulated in the process. Overall, this study highlights the ability of tumor-derived secretory factors to cause WAT browning and energy wasting. WAT browning is catastrophic in the context of cancer because it accelerates energy wasting, so targeting these factors might block WAT browning–associated energy wasting in patients with cachexia. FJ

ACKNOWLEDGMENTS

The authors thank Dr. Patrick Seale (University of Pennsylvania, Philadelphia, PA, USA) for providing control and *Prdm16* luciferase reporter vectors, and Dr. Mark Christian (University of Warwick, Coventry, United Kingdom) for providing *Ucp1* luciferase vector. The authors thank Jinling Yuan (Georgia Cancer Center) for animal care and Georgia Cancer Center Small Animal Imaging Resource (Augusta, GA, USA) for technical help with multispectral optical imaging. The authors thank Dr. Rhea-Beth Markowitz (Augusta University) for reviewing and editing the manuscript. This research is supported by the U.S. National Institutes of Health, National Institute of Diabetes and Digestive and Kidney Diseases (Grant DP2DK105565 to A.S.). The authors declare no conflicts of interest.

AUTHOR CONTRIBUTIONS

S. Elattar and M. Dimri performed experiments and collected and analyzed data; A. Satyanarayana supervised

the study; and A. Satyanarayana and S. Elattar analyzed and interpreted the data and wrote the manuscript.

REFERENCES

1. Morley, J. E., Thomas, D. R., and Wilson, M. M. (2006) Cachexia: pathophysiology and clinical relevance. *Am. J. Clin. Nutr.* **83**, 735–743
2. Tisdale, M. J. (2002) Cachexia in cancer patients. *Nat. Rev. Cancer* **2**, 862–871
3. Fearon, K. C., Glass, D. J., and Guttridge, D. C. (2012) Cancer cachexia: mediators, signaling, and metabolic pathways. *Cell Metab.* **16**, 153–166
4. Van Hall, G., Steensberg, A., Fischer, C., Keller, C., Møller, K., Moseley, P., and Pedersen, B. K. (2008) Interleukin-6 markedly decreases skeletal muscle protein turnover and increases nonmuscle amino acid utilization in healthy individuals. *J. Clin. Endocrinol. Metab.* **93**, 2851–2858
5. Li, Y. P., Schwartz, R. J., Waddell, I. D., Holloway, B. R., and Reid, M. B. (1998) Skeletal muscle myocytes undergo protein loss and reactive oxygen-mediated NF-κB activation in response to tumor necrosis factor α. *FASEB J.* **12**, 871–880
6. Strassmann, G., Fong, M., Kenney, J. S., and Jacob, C. O. (1992) Evidence for the involvement of interleukin 6 in experimental cancer cachexia. *J. Clin. Invest.* **89**, 1681–1684
7. Petruzzelli, M., Schweiger, M., Schreiber, R., Campos-Olivas, R., Tsoli, M., Allen, J., Swarbrick, M., Rose-John, S., Rincon, M., Robertson, G., Zechner, R., and Wagner, E. F. (2014) A switch from white to brown fat increases energy expenditure in cancer-associated cachexia. *Cell Metab.* **20**, 433–447
8. Argilés, J. M., Busquets, S., Stemmler, B., and López-Soriano, F. J. (2014) Cancer cachexia: understanding the molecular basis. *Nat. Rev. Cancer* **14**, 754–762
9. Cannon, B., and Nedergaard, J. (2004) Brown adipose tissue: function and physiological significance. *Physiol. Rev.* **84**, 277–359
10. Wang, Q. A., Tao, C., Gupta, R. K., and Scherer, P. E. (2013) Tracking adipogenesis during white adipose tissue development, expansion and regeneration. *Nat. Med.* **19**, 1338–1344
11. Seale, P., Bjork, B., Yang, W., Kajimura, S., Chin, S., Kuang, S., Scimè, A., Devarakonda, S., Conroe, H. M., Erdjument-Bromage, H., Tempst, P., Rudnicki, M. A., Beier, D. R., and Spiegelman, B. M. (2008) PRDM16 controls a brown fat/skeletal muscle switch. *Nature* **454**, 961–967
12. Seale, P., Kajimura, S., Yang, W., Chin, S., Rohas, L. M., Uldry, M., Tavernier, G., Langin, D., and Spiegelman, B. M. (2007) Transcriptional control of brown fat determination by PRDM16. *Cell Metab.* **6**, 38–54
13. Rajakumari, S., Wu, J., Ishibashi, J., Lim, H. W., Giang, A. H., Won, K. J., Reed, R. R., and Seale, P. (2013) EBF2 determines and maintains brown adipocyte identity. *Cell Metab.* **17**, 562–574
14. Kajimura, S., Seale, P., Kubota, K., Lunsford, E., Frangioni, J. V., Gygi, S. P., and Spiegelman, B. M. (2009) Initiation of myoblast to brown fat switch by a PRDM16-C/EBP-β transcriptional complex. *Nature* **460**, 1154–1158
15. Seale, P., Conroe, H. M., Estall, J., Kajimura, S., Frontini, A., Ishibashi, J., Cohen, P., Cinti, S., and Spiegelman, B. M. (2011) Prdm16 determines the thermogenic program of subcutaneous white adipose tissue in mice. *J. Clin. Invest.* **121**, 96–105
16. Stine, R. R., Shapira, S. N., Lim, H. W., Ishibashi, J., Harms, M., Won, K. J., and Seale, P. (2015) EBF2 promotes the recruitment of beige adipocytes in white adipose tissue. *Mol. Metab.* **5**, 57–65
17. Harms, M., and Seale, P. (2013) Brown and beige fat: development, function and therapeutic potential. *Nat. Med.* **19**, 1252–1263
18. Burgi, W., and Schmid, K. (1961) Preparation and properties of Zn-α_2-glycoprotein of normal human plasma. *J. Biol. Chem.* **236**, 1066–1074
19. Hale, L. P., Price, D. T., Sanchez, L. M., Demark-Wahnefried, W., and Madden, J. F. (2001) Zinc α-2-glycoprotein is expressed by malignant prostatic epithelium and may serve as a potential serum marker for prostate cancer. *Clin. Cancer Res.* **7**, 846–853
20. Díez-Itza, I., Sánchez, L. M., Allende, M. T., Vizoso, F., Ruibal, A., and López-Otín, C. (1993) Zn-α_2-glycoprotein levels in breast cancer cytosols and correlation with clinical, histological and biochemical parameters. *Eur. J. Cancer* **29A**, 1256–1260
21. Bondar, O. P., Barnidge, D. R., Klee, E. W., Davis, B. J., and Klee, G. G. (2007) LC-MS/MS quantification of Zn-α2 glycoprotein: a potential serum biomarker for prostate cancer. *Clin. Chem.* **53**, 673–678
22. Abdul-Rahman, P. S., Lim, B. K., and Hashim, O. H. (2007) Expression of high-abundance proteins in sera of patients with endometrial and cervical cancers: analysis using 2-DE with silver staining and lectin detection methods. *Electrophoresis* **28**, 1989–1996
23. Bing, C., Bao, Y., Jenkins, J., Sanders, P., Manieri, M., Cinti, S., Tisdale, M. J., and Trayhurn, P. (2004) Zinc-α2-glycoprotein, a lipid mobilizing factor, is expressed in adipocytes and is up-regulated in mice with cancer cachexia. *Proc. Natl. Acad. Sci. USA* **101**, 2500–2505
24. Taylor, D. D., Gercel-Taylor, C., Jenis, L. G., and Devereux, D. F. (1992) Identification of a human tumor-derived lipolysis-promoting factor. *Cancer Res.* **52**, 829–834
25. Mracek, T., Ding, Q., Tzanavari, T., Kos, K., Pinkney, J., Wilding, J., Trayhurn, P., and Bing, C. (2010) The adipokine zinc-α2-glycoprotein (ZAG) is downregulated with fat mass expansion in obesity. *Clin. Endocrinol. (Oxf.)* **72**, 334–341
26. Mracek, T., Gao, D., Tzanavari, T., Bao, Y., Xiao, X., Stocker, C., Trayhurn, P., and Bing, C. (2010) Downregulation of zinc-α2-glycoprotein in adipose tissue and liver of obese *ob/ob* mice and by tumour necrosis factor-α in adipocytes. *J. Endocrinol.* **204**, 165–172
27. Russell, S. T., Hirai, K., and Tisdale, M. J. (2002) Role of β3-adrenergic receptors in the action of a tumour lipid mobilizing factor. *Br. J. Cancer* **86**, 424–428
28. Patil, M., Sharma, B. K., Elattar, S., Chang, J., Kapil, S., Yuan, J., and Satyanarayana, A. (2017) Id1 promotes obesity by suppressing brown adipose thermogenesis and white adipose browning. *Diabetes* **66**, 1611–1625
29. Satyanarayana, A., Klarmann, K. D., Gavrilova, O., and Keller, J. R. (2012) Ablation of the transcriptional regulator *Id1* enhances energy expenditure, increases insulin sensitivity, and protects against age and diet induced insulin resistance, and hepatosteatosis. *FASEB J.* **26**, 309–323
30. Kir, S., White, J. P., Kleiner, S., Kazak, L., Cohen, P., Baracos, V. E., and Spiegelman, B. M. (2014) Tumour-derived PTH-related protein triggers adipose tissue browning and cancer cachexia. *Nature* **513**, 100–104
31. Ohno, H., Shinoda, K., Spiegelman, B. M., and Kajimura, S. (2012) PPARγ agonists induce a white-to-brown fat conversion through stabilization of PRDM16 protein. *Cell Metab.* **15**, 395–404
32. Wu, J., Boström, P., Sparks, L. M., Ye, L., Choi, J. H., Giang, A. H., Khandekar, M., Virtanen, K. A., Nuutila, P., Schaart, G., Huang, K., Tu, H., van Marken Lichtenbelt, W. D., Hoeks, J., Enerbäck, S., Schrauwen, P., and Spiegelman, B. M. (2012) Beige adipocytes are a distinct type of thermogenic fat cell in mouse and human. *Cell* **150**, 366–376
33. Vegiopoulos, A., Müller-Decker, K., Strzoda, D., Schmitt, I., Chichelnitskiy, E., Ostertag, A., Berriel Diaz, M., Rozman, J., Hrabe de Angelis, M., Nüsing, R. M., Meyer, C. W., Wahli, W., Klingenspor, M., and Herzig, S. (2010) Cyclooxygenase-2 controls energy homeostasis in mice by de novo recruitment of brown adipocytes. *Science* **328**, 1158–1161
34. Rodeheffer, M. S., Birsoy, K., and Friedman, J. M. (2008) Identification of white adipocyte progenitor cells in vivo. *Cell* **135**, 240–249
35. Aune, U. L., Ruiz, L., and Kajimura, S. (2013) Isolation and differentiation of stromal vascular cells to beige/brite cells. *J. Vis. Exp.* **73**, e50191
36. Yusuf, B., Gopurappilly, R., Dadheech, N., Gupta, S., Bhonde, R., and Pal, R. (2013) Embryonic fibroblasts represent a connecting link between mesenchymal and embryonic stem cells. *Dev. Growth Differ.* **55**, 330–340
37. Hansen, J. B., Jørgensen, C., Petersen, R. K., Hallenborg, P., De Matteis, R., Bøye, H. A., Petrovic, N., Enerbäck, S., Nedergaard, J., Cinti, S., te Riele, H., and Kristiansen, K. (2004) Retinoblastoma protein functions as a molecular switch determining white versus brown adipocyte differentiation. *Proc. Natl. Acad. Sci. USA* **101**, 4112–4117
38. Rosen, E. D., and MacDougald, O. A. (2006) Adipocyte differentiation from the inside out. *Nat. Rev. Mol. Cell Biol.* **7**, 885–896
39. Rosen, E. D., Hsu, C. H., Wang, X., Sakai, S., Freeman, M. W., Gonzalez, F. J., and Spiegelman, B. M. (2002) C/EBPα induces adipogenesis through PPARγ: a unified pathway. *Genes Dev.* **16**, 22–26
40. Lowell, B. B. (1999) An essential regulator of adipogenesis and modulator of fat cell function: PPARγ. *Cell* **99**, 239–242
41. Coussens, L. M., and Werb, Z. (2002) Inflammation and cancer. *Nature* **420**, 860–867
42. Janssen, S. P., Gayan-Ramirez, G., Van den Bergh, A., Herijgers, P., Maes, K., Verbeken, E., and Decramer, M. (2005) Interleukin-6 causes

myocardial failure and skeletal muscle atrophy in rats. *Circulation* **111**, 996–1005
43. Busquets, S., Sanchís, D., Alvarez, B., Ricquier, D., López-Soriano, F. J., and Argilés, J. M. (1998) In the rat, tumor necrosis factor α administration results in an increase in both UCP2 and UCP3 mRNAs in skeletal muscle: a possible mechanism for cytokine-induced thermogenesis? *FEBS Lett.* **440**, 348–350
44. Yeaman, S. J. (2004) Hormone-sensitive lipase—new roles for an old enzyme. *Biochem. J.* **379**, 11–22
45. Cypess, A. M., Weiner, L. S., Roberts-Toler, C., Franquet Elía, E., Kessler, S. H., Kahn, P. A., English, J., Chatman, K., Trauger, S. A., Doria, A., and Kolodny, G. M. (2015) Activation of human brown adipose tissue by a β3-adrenergic receptor agonist. *Cell Metab.* **21**, 33–38
46. Petrovic, N., Walden, T. B., Shabalina, I. G., Timmons, J. A., Cannon, B., and Nedergaard, J. (2010) Chronic peroxisome proliferator-activated receptor γ (PPARγ) activation of epididymally derived white adipocyte cultures reveals a population of thermogenically competent, UCP1-containing adipocytes molecularly distinct from classic brown adipocytes. *J. Biol. Chem.* **285**, 7153–7164
47. Cao, L., Choi, E. Y., Liu, X., Martin, A., Wang, C., Xu, X., and During, M. J. (2011) White to brown fat phenotypic switch induced by genetic and environmental activation of a hypothalamic-adipocyte axis. *Cell Metab.* **14**, 324–338
48. Sanders, P. M., and Tisdale, M. J. (2004) Effect of zinc-α_2-glycoprotein (ZAG) on expression of uncoupling proteins in skeletal muscle and adipose tissue. *Cancer Lett.* **212**, 71–81
49. Puigserver, P., Adelmant, G., Wu, Z., Fan, M., Xu, J., O'Malley, B., and Spiegelman, B. M. (1999) Activation of PPARγ coactivator-1 through transcription factor docking. *Science* **286**, 1368–1371
50. Lin, J., Wu, P. H., Tarr, P. T., Lindenberg, K. S., St-Pierre, J., Zhang, C. Y., Mootha, V. K., Jäger, S., Vianna, C. R., Reznick, R. M., Cui, L., Manieri, M., Donovan, M. X., Wu, Z., Cooper, M. P., Fan, M. C., Rohas, L. M., Zavacki, A. M., Cinti, S., Shulman, G. I., Lowell, B. B., Krainc, D., and Spiegelman, B. M. (2004) Defects in adaptive energy metabolism with CNS-linked hyperactivity in *PGC-1α* null mice. *Cell* **119**, 121–135
51. Puigserver, P., Wu, Z., Park, C. W., Graves, R., Wright, M., and Spiegelman, B. M. (1998) A cold-inducible coactivator of nuclear receptors linked to adaptive thermogenesis. *Cell* **92**, 829–839
52. Bing, C., Russell, S. T., Beckett, E. E., Collins, P., Taylor, S., Barraclough, R., Tisdale, M. J., and Williams, G. (2002) Expression of uncoupling proteins-1, -2 and -3 mRNA is induced by an adenocarcinoma-derived lipid-mobilizing factor. *Br. J. Cancer* **86**, 612–618
53. Wargent, E. T., O'Dowd, J. F., Zaibi, M. S., Gao, D., Bing, C., Trayhurn, P., Cawthorne, M. A., Arch, J. R., and Stocker, C. J. (2013) Contrasts between the effects of zinc-α_2-glycoprotein, a putative $\beta_{3/2}$-adrenoceptor agonist and the $\beta_{3/2}$-adrenoceptor agonist BRL35135 in C57Bl/6 (*ob/ob*) mice. *J. Endocrinol.* **216**, 157–168
54. Bayliss, T. J., Smith, J. T., Schuster, M., Dragnev, K. H., and Rigas, J. R. (2011) A humanized anti-IL-6 antibody (ALD518) in non-small cell lung cancer. *Expert Opin. Biol. Ther.* **11**, 1663–1668

Received for publication December 7, 2017.
Accepted for publication March 12, 2018.